J Solid State Electrochem (2001) 5: 437–449
DOI 10.1007/s100080000183

ORIGINAL PAPER

Angela Šurca Vuk · Boris Orel · Goran Dražič

# IR spectroelectrochemical studies of $Fe_2V_4O_{13}$, $FeVO_4$ and $InVO_4$ thin films obtained via sol-gel synthesis

Received: 3 September 2000 / Accepted: 21 November 2000 / Published online: 3 July 2001


**Abstract** In this paper we generalize the IR spectroscopic properties of $M^{3+}VO_4$ (M = Fe, In) orthovanadate and $Fe_2V_4O_{13}$ films. The films were prepared using the sol-gel synthesis route from $M^{3+}$ nitrates and vanadium oxoisopropoxide. The vibrational bands in the IR absorbance spectra of the films are classified in terms of terminal V-O stretching (1050–880 $cm^{-1}$), bridging V-O···Fe and V···O···Fe stretching (880–550 $cm^{-1}$), mixed V-O-V deformations and Fe-O stretching (< 550 $cm^{-1}$) modes. Ex situ IR spectra of films were measured after consecutive charging/discharging to various intercalation coefficients $x$ and correlated to the current peaks in the cyclic voltammetry curves measured in 1 M $LiClO_4$/propylene carbonate electrolyte. We classified the ex situ IR spectra of charged/discharged films according to their vibrational band changes. The results reveal that, for small values of the intercalation coefficient, crystalline $FeVO_4$, $InVO_4$ and $Fe_2V_4O_{13}$ films exhibit a simultaneous decrease in the intensity of all IR bands while the band frequencies remain unaffected. For the higher intercalation levels, IR mode frequencies are shifted, signaling the presence of reduced vanadium. Further charging leads to an amorphization of the film structure, which was established from the similarity of the IR spectra of charged films with those of amorphous films prepared at lower annealing temperatures. The results confirm that ex situ IR spectroelectrochemical measurement is an effective way to assess the structural changes in films with different levels of intercalation.

Presented at the international conference "Solid State Chemistry 2000", 3–8 September 2000, Prague, Czech Republic

A. Šurca Vuk · B. Orel (✉)
National Institute of Chemistry,
Hajdrihova 19, 1000 Ljubljana, Slovenia
E-mail: boris.orel@ki.si
Tel.: +386-1-4760200
Fax: +386-1-4259244

G. Dražič
Josef Stefan Institute, Jamova 39,
1000 Ljubljana, Slovenia

**Keywords** Vanadates · Infrared spectroelectrochemistry · Electrochromism · Sol-gel synthesis · Thin films

## Introduction

IR spectroelectrochemical studies [1, 2, 3] have been extensively used for the investigation of the surface species formed on various metals [4, 5, 6], for example lithium [7, 8, 9, 10], and on different cathode materials for lithium rechargeable batteries [11, 12]. The external reflection-absorption technique, performed at a near-grazing incidence angle (NGIA, 80°) with the p-polarized IR beam, was successfully employed for the detection of species in the passivation layer of electrodes [8, 9, 13]. This method performs well when surface species need to be established, but becomes tedious when interpreting IR spectra of species which form due to the insertion of lithium inside the electrode film [14, 15]. Namely, the spectral response corresponds to the longitudinal optical excitations (LO modes) and the absorption spectra (transversal optical modes, TO modes) can be obtained only after extensive calculations, for which the optical constants ($n$ and $k$) of the phonon modes of the electrode films are required [16, 17, 18].

Alternatively, attenuated total reflection (ATR) spectroelectrochemical measurement [1, 19, 20, 21] gives directly the TO modes of species formed either on the surface or inside the electrode film. The main drawback is the need for suitable ATR materials which have a high refractive index and allow the deposition of films at high temperatures (500 °C). In addition, to ensure electrical contact a thin conductive layer (usually Pt) should be deposited on the ATR crystal before the deposition of the investigated electrode film, which diminishes the intensity of the bands in the in situ ATR spectra. The ATR technique was successfully applied to studies of organic electrically conductive polymers (i.e. polyaniline [19]) and surface species on lithium electrodes [7, 10]. It seems that this technique is more

suitable for organic thin films with a smaller dispersion than for inorganic films [22].

In our investigations of the intercalation/deintercalation properties of different electrochromic films, we used in situ NGIA IR and ex situ IR transmission spectroelectrochemical techniques [14, 15, 23, 24, 25, 26, 27, 28, 29]. Although the ex situ transmission technique gives the TO modes of thin electrode films directly, it is nearly impossible to make in situ measurements because of the very high absorption of the electrolyte. The ex situ IR transmission technique was successfully applied to thin films which retain their charge after being removed from the electrochemical cell. Cleaning of the films removes traces of the electrolyte and high-quality IR spectra are obtained. $CO_2$ surface species eventually form during the manipulation in air but can be easily identified in the spectra.

Generally, IR spectra of initial, charged and discharged electrochromic films are needed to assess the presence of reduced transition metal species, to obtain information about the irreversible retention of lithium ions in the film structure and to determine the amount of charge needed to attain the change of the crystal modification or amorphization of the crystalline films. The identification of reduced metal species can be inferred from the vibrational mode shifts which appear in charged spectra. The IR spectra of model compounds with known oxidation states (lower oxides, for example) are helpful. In certain cases the polaron absorption is identified [14, 15]. A comparison of discharged and initial spectra gives evidence about the reversibility of charging and the appearance of new $Li^+$-O modes reveals the irreversible lithiation. The amorphization of films can be assessed from the similarities between the IR spectra of discharged films and the initial spectra of films prepared at lower temperatures, for which transmission electron microscope (TEM) and X-ray diffraction (XRD) measurements confirm the amorphous structure.

The present investigation is a continuation of electrochromic and structural studies of $M^{3+}VO_4$ ($M^{3+}$ = Ce, Fe, In) orthovanadate and $Fe_2V_4O_{13}$ films prepared via sol-gel synthesis and dip-coating deposition [23, 25, 26, 27, 28, 29]. $InVO_4$ and $FeVO_4$ attracted our interest because the powders are able to take up a large amount of lithium ions ($x = 10$–$12$) when charged close to the potential of Li [30]. A complete discharge is not possible and a certain amount of lithium remains in the structure ($x = 2$–$4$), leading to the amorphization of the initially crystalline powders. Since charging/discharging becomes reversible after the first few cycles, $FeVO_4$ and $InVO_4$ were proposed as anodes for rechargeable lithium batteries.

In and Fe vanadate powders have been prepared in different ways [30, 31, 32, 33, 34, 35, 36], including wet chemistry (chemie douce) techniques [30, 33, 34, 35, 36]. Among the latter techniques, a dissolution-reprecipitation route employed a long stirring of a mixture of $M^{3+}$ nitrates ($M^{3+}$ = In, Fe) and vanadic acid or $V_2O_5.1.6H_2O$ [33, 34, 35]. This route was later generalized for the synthesis of various mono-, di- and trivalent vanadate powders [36]. Because the technique is based on aqueous solutions, it is less suitable for the dip-coating deposition of films. Films obtained from aqueous colloidal solutions are of poor optical quality and their deposition requires the use of surfactants. For these reasons we prepared alcoholic sols based on vanadium oxoisopropoxide and $M^{3+}$ nitrate precursors [25, 26, 27, 28, 29].

In our previous publications we gave detailed reports of the electrochromic properties of $CeVO_4$ [23], $Fe_2V_4O_{13}$ [25, 26], $FeVO_4$ [27] and $InVO_4$ [28, 29] crystalline films. Our results show that all the films have a high ion-storage capacity (20–30 mC $cm^{-2}$) and small variations in photopic transmittance ($\Delta T_{vis} < 0.10$). Accordingly, these films are potential counter-electrodes in electrochromic (smart) windows.

The main purpose of this study is to generalize the IR spectroscopic behaviour of $M^{3+}VO_4$ ($M^{3+}$ = Fe, In) orthovanadate and $Fe_2V_4O_{13}$ films [23, 25, 26, 27, 28, 29]. First, we present cyclic voltammograms (CVs) of the crystalline $FeVO_4$, $Fe_2V_4O_{13}$ and $InVO_4$ films. The insertion of lithium ions is assessed with the intercalation coefficient $x$ (per V atom). Ex situ IR spectra of films charged to different levels are shown and a detailed description is given for crystalline $FeVO_4$ films. In addition, the IR vibrational band changes are correlated with the appearance of current peaks in the CVs. Particular attention is also given to the spectral features that signal the retention of lithium ions in the film structure and its transformation to an amorphous phase.

## Experimental

$FeVO_4$ and $Fe_2V_4O_{13}$ films were prepared using the sol-gel synthesis route. First, a $Fe(NO_3)_3.9H_2O$ precursor was dissolved in *n*-propanol. Vanadium oxoisopropoxide was then added to the solution in molar ratios of Fe:V = 1:1 and 1:2. The sols, dark red in colour, were stirred for 1 h, after which the thin films were deposited by the dip-coating technique with a pulling velocity of 10 cm $min^{-1}$. The $FeVO_4$ films were obtained after heating at 500 °C (1 h), while $Fe_2V_4O_{13}$ formed at 400 °C (1 h). The same preparation route was used to obtain $InVO_4$ films. Vanadium oxoisopropoxide was added in a molar ratio of In:V = 1:1 to a solution of $In(NO_3)_3.5H_2O$ in *n*-propanol (yellow-orange sol) and the deposited films were heated at 500 °C for 1 h. Film thickness was determined using a Profilometer Talysurf (Taylor Hobson).

Fragments of the Fe/V (1:1) oxide film (300 °C) were prepared by gentle scratching of the film's surface and subsequent transfer to a hollow-carbon coated Cu grid for TEM examination. Cross sections of the Fe/V (1:1) oxide film (400 and 500 °C) on a $<Si>/SiO_2/TiO_2/Pt$ substrate were prepared using a Gatan cross-sectional TEM specimen preparation kit. After mechanical thinning and dimpling, ion milling using 3.8 keV argon ions were used. To prevent degradation, samples were cooled with liquid nitrogen during the final stages of the ion erosion process. Samples were examined using a Jeol 2000 FX TEM, operating at 200 kV. The chemical composition of the phases was determined using a Link AN-10000 energy dispersive X-ray spectroscopy (EDXS) system with an ultra-thin window Si(Li) detector, connected to the TEM. To determine the phases present in the film, we simulated electron diffraction patterns using the Electron Microscopy Simulation (EMS) program package [37] for various mean crystallite sizes.

CV curves were obtained using an EG&G Par 273 potentiostat/galvanostat. Measurements were made in a three-electrode cell using a thin film as the working electrode, a Pt rod as the counter electrode and a modified Ag/AgCl electrode as reference. The electrolyte was 1 M $LiClO_4$/propylene carbonate (PC). Ex situ IR absorbance spectra (TO modes) were measured using a Perkin-Elmer System 2000. Vanadate films were deposited on double-sided polished Si wafers with an electrical resistivity of 10–20 Ω cm. Ex situ IR spectra were obtained after the films were galvanostatically or potentiostatically charged/discharged. In-Ga alloy was applied to the Si wafers to increase the conductivity of the electrical contact.

## Results

### TEM measurements

The TEM micrograph of the $FeVO_4$ film (300 °C) in a central dark field (CDF) exhibits mainly an amorphous structure (Fig. 1A), with larger areas of bright contrast (up to 50 nm) which correspond to a triclinic $FeVO_4$-I phase [32]. Smaller nanocrystallites of size 1–2 nm and 5 nm were identified as an orthorhombic $FeVO_4$-II (high-pressure [38]) phase. At higher temperature (400 °C) the films are composed of grains up to 50 nm in size (not shown). The selected area electron diffraction (SAED) pattern reveals that both $FeVO_4$-I and $FeVO_4$-II phases are present. Electrochromic properties of these films (400 °C) have been reported elsewhere [27]. The TEM micrograph and SAED pattern of a $FeVO_4$ film prepared at 500 °C reveal grains with dimensions of 50–80 nm (Fig. 1B). EDXS shows that the chemical composition across the film is uniform. Grains are randomly oriented and correspond to the monoclinic $FeVO_4$-I phase [32].

TEM micrographs and XRD data of the $Fe_2V_4O_{13}$ [25, 26], $FeVO_4$ (400 °C) [27] and $InVO_4$ [28] films have already been reported and the results are summarized in Table 1. The $Fe_2V_4O_{13}$ films (400 °C) consist predominantly of a monoclinic $Fe_2V_4O_{13}$ phase [39] with very fine-grained orthorhombic $FeVO_4$-II [38]. Similarly,

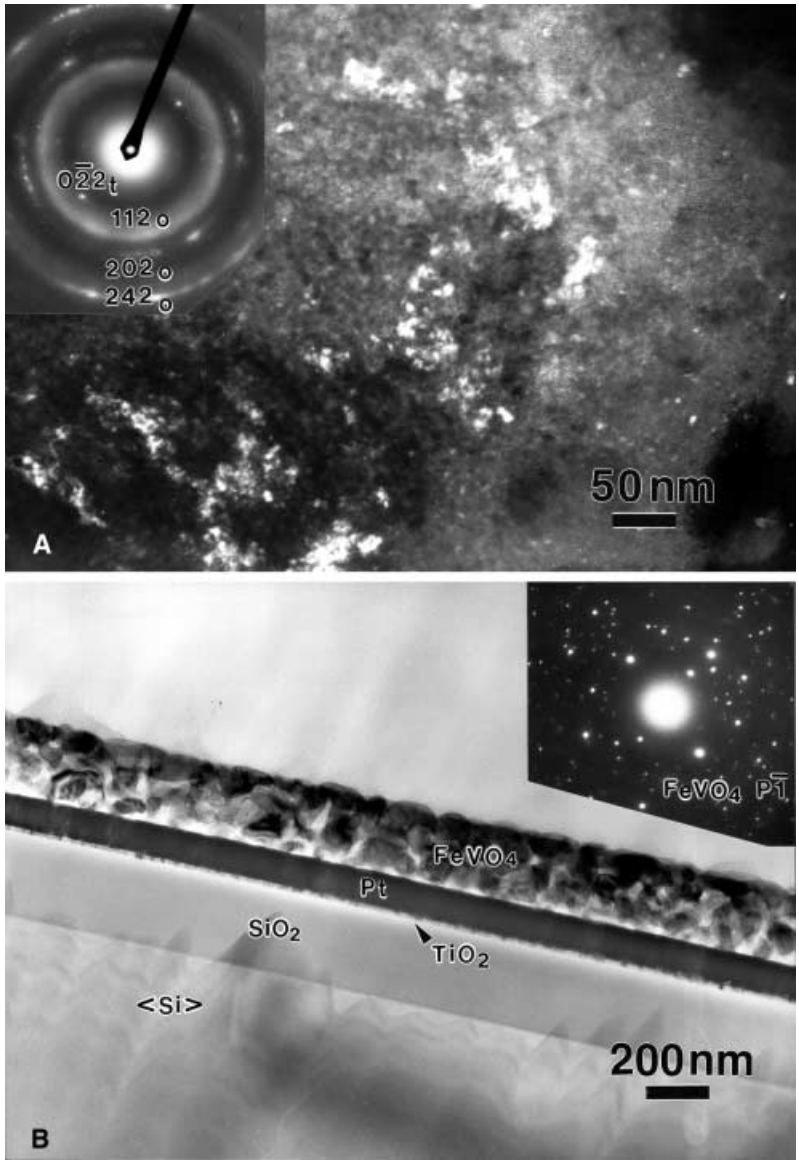


**Fig. 1** TEM micrographs and corresponding selected area electron diffraction patterns of thin Fe/V (1:1) oxide films prepared at **A** 300 °C (dark field) and **B** 500 °C

**Table 1** Presentation of the development of the structure of $FeVO_4$, $Fe_2V_4O_{13}$ and $InVO_4$ films

| Type of film | $T_h$ (°C)[a] | Structure of film | Ref |
|---|---|---|---|
| $FeVO_4$ | 300 | TEM: predominant amorphous phase, $FeVO_4$-II (1–2 nm), $FeVO_4$-I (50 nm, few grain formations in SAED); XRD: unknown phase | [26] |
| | 400 | TEM: crystalline, $FeVO_4$-I and $FeVO_4$-II (~50 nm), homogeneous composition (EDXS); XRD: mixed I and II phases | [26, 27] |
| | 500 | TEM: crystalline $FeVO_4$-I (50–80 nm), randomly oriented grains, homogeneous composition (EDXS) | – |
| $Fe_2V_4O_{13}$ | 300 | TEM: predominant amorphous phase, $FeVO_4$-II (1–2 nm); XRD: weakly expressed $Fe_2V_4O_{13}$ | [26] |
| | 400 | TEM: predominant crystalline $Fe_2V_4O_{13}$ (50 nm), $FeVO_4$-II (5 nm), amorphous phase could not be excluded, binodal distribution of grains; XRD: $Fe_2V_4O_{13}$ and $FeVO_4$-II | [25, 26] |
| | 500 | Not possible to prepare films with optical quality | – |
| $InVO_4$ | 300 | TEM: predominant amorphous phase, $InVO_4$-III (1 nm), crystallization in e-beam | [28] |
| | 500 | XRD: $InVO_4$-I (predominant), $InVO_4$-III (< 20%) | [28] |
| $CeVO_4$ | 400 | XRD: crystalline $CeVO_4$ (wakefieldite) | [23] |

[a] $T_h$: temperature of heating

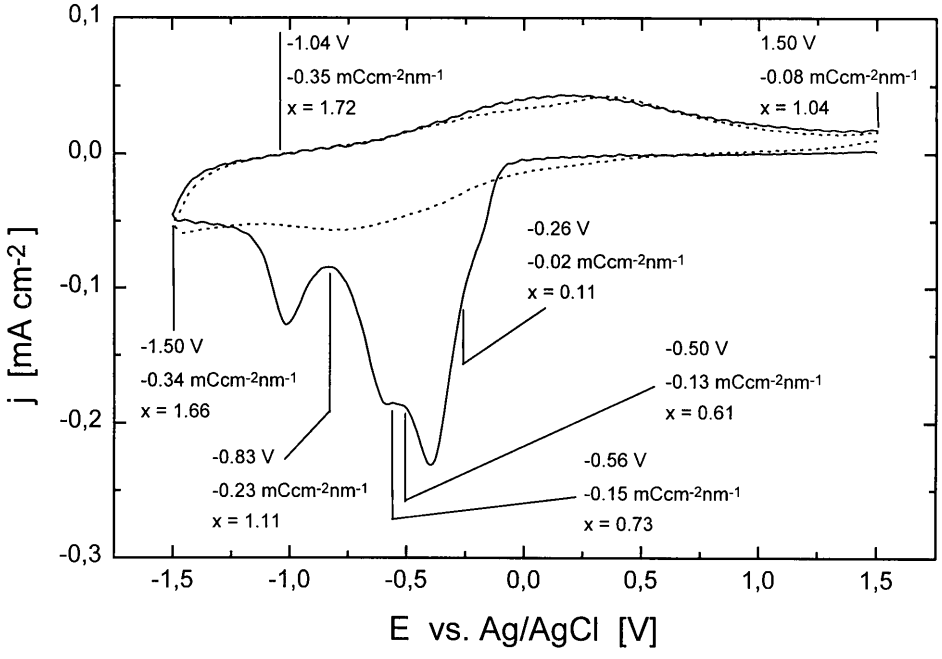


**Fig. 2** CV response of a $FeVO_4$ film (500 °C): first cycle (*solid line*) and second cycle (*dotted line*). Charge per thickness $Qd^{-1}$ and insertion coefficient $x$ are given for the first cycle

crystalline $InVO_4$ films (500 °C) consist predominantly of the monoclinic $InVO_4$-I phase [35] with a small amount (< 20%) of the orthorhombic $InVO_4$-III phase [31].

## Electrochemical measurements

The investigated $FeVO_4$ and $Fe_2V_4O_{13}$ films were cycled in the potential range from 1.5 to –1.5 V vs. Ag/AgCl (Figs. 2, 3), while the $InVO_4$ films were tested between 1.6 and –1.6 V vs. Ag/AgCl (Fig. 4). The scan speed used was 5 mV $s^{-1}$. The characteristic feature of the $FeVO_4$ and $Fe_2V_4O_{13}$ films is that the first cathodic cycle differs considerably from the second; however, the anodic cycles are similar. Such behaviour is observed for $V_2O_5$ crystalline films cycled in the same potential range and was explained by the amorphization of the film structure [14, 15]. The inserted charge per thickness $Qd^{-1}$ obtained by integration of the peaks in the first cathodic scan of both crystalline Fe vanadates is high, i.e. –0.35 mC $cm^{-2}$ $nm^{-1}$ for $FeVO_4$ and –0.71 mC $cm^{-2}$ $nm^{-1}$ for $Fe_2V_4O_{13}$ films, resulting in intercalation coefficients ($x$ per V atom) of $x = 1.72$ ($FeVO_4$) and 3.07 ($Fe_2V_4O_{13}$) (Figs. 2, 3; Table 2). The $Qd^{-1}$ value determined for $InVO_4$ (500 °C) films (Fig. 4) is smaller, i.e. –0.19 mC $cm^{-2}$ $nm^{-1}$ (Table 2).

The peaks in the CV of the $FeVO_4$ film (Fig. 2) can be correlated with the inflections observed in voltage versus composition curves of powders [30]. A good match is

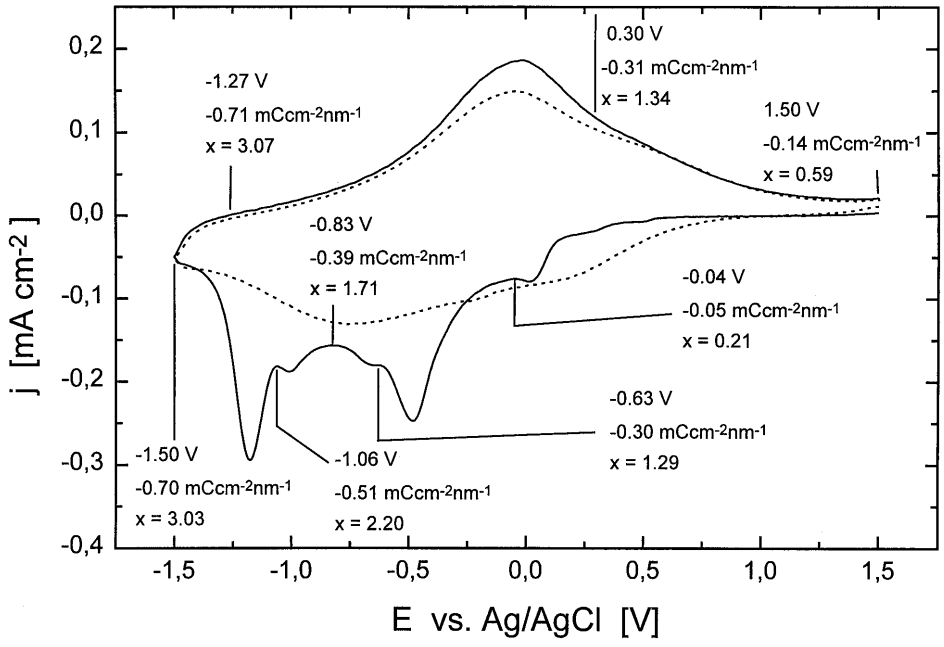


**Fig. 3** CV response of a $Fe_2V_4O_{13}$ film (400 °C): first cycle (*solid line*) and second cycle (*dotted line*). Charge per thickness $Qd^{-1}$ and insertion coefficient $x$ are given for the first cycle

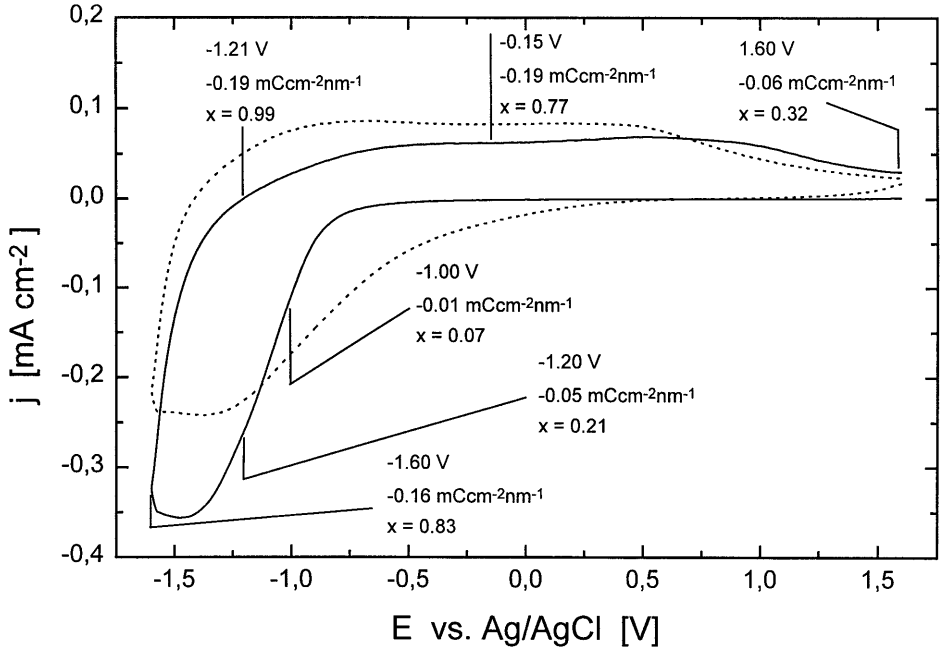


**Fig. 4** CV response of an $InVO_4$ film (500 °C): first cycle (*solid line*) and second cycle (*dotted line*). Charge per thickness $Qd^{-1}$ and insertion coefficient $x$ are given for the first cycle

noted also for the current peak at –1.45 V vs. Ag/AgCl in the CV of the predominantly monoclinic $InVO_4$-I film (Fig. 4) and the position of the $dx/dV$ peak observed for powders by Denis et al. [30]. The CVs of all investigated films show irreversible lithiation. The highest retention of lithium is noted for $Fe_2V_4O_{13}$ (–0.14 mC $cm^{-2}$ $nm^{-1}$); $FeVO_4$ follows with –0.08 mC $cm^{-2}$ $nm^{-1}$, while the charge which remains in crystalline $InVO_4$ films reaches –0.06 mC $cm^{-2}$ $nm^{-1}$ (Figs. 2, 3, 4; Table 2). Irreversible lithiation is in accordance with voltage versus composition curves of $FeVO_4$ and $InVO_4$ powders [30], which reveal that charging to low potentials vs. Li (i.e. 0.02 V vs. Li) leads to intercalation coefficients of $x = 8$ for $FeVO_4$ and $x = 9$ for $InVO_4$. Complete delithiation was not obtained during discharging to 3.5 V vs. Li.

## IR spectra of films

The IR and Raman spectra of $FeVO_4$ films and powders obtained under various heating conditions have been studied and the vibrational bands assigned [25, 27]. Inspection of the IR spectra of $FeVO_4$ films prepared at 300, 400 and 500 °C (Fig. 5) shows an increase in the number of bands with temperature. This agrees with the structural changes already established by TEM and

**Table 2** Intercalation properties of crystalline $Fe_2V_4O_{13}$, $FeVO_4$ and $InVO_4$ films during ex situ IR and cyclic voltammetry measurements

| $Fe_2V_4O_{13}$ film; 400 °C, 60 min; $d = 70$ nm | | | | | | | | | | | | | | |
|---|---|---|---|---|---|---|---|---|---|---|---|---|---|---|
| Ex situ IR absorbance spectra | | | | | | | | | CV, SR = 5 mV $s^{-1}$ | | | | | |
| Techn[a] | Cycle | $E$ | $i$ | $t$ | $Q_{ins}$ | $Q_{ins}d^{-1}$ | $\rho$ | $x'$ | $x$ | $E$ | $Q_{ins}$ | $Q_{ins}d^{-1}$ | $x'$ | $x$ |
| CC | 1 | –1.50 | – | 120 | –4.3 | –0.06 | 3.122 | 1.07 | 0.27 | –0.04 | –3.4 | –0.05 | 0.84 | 0.21 |
| | 2 | –1.50 | | 120 | –8.9 | –0.13 | | 2.21 | 0.55 | –0.63 | –20.8 | –0.30 | 5.16 | 1.29 |
| | 6 | –1.50 | | 480 | –9.0 | –0.13 | | 2.21 | 0.55 | | | | | |
| | 7 | –2.00 | | 1680 | –11.9 | –0.17 | | 2.95 | 0.74 | –0.83 | –27.5 | –0.39 | 6.83 | 1.71 |
| | 8 | –3.00 | | 480 | –23.3 | –0.33 | | 5.77 | 1.44 | –1.06 | –35.5 | –0.51 | 8.80 | 2.20 |
| CE | 4 | – | 23.8 | 1680 | –40.0 | –0.57 | | 9.93 | 2.48 | –1.50 | –48.7 | –0.70 | 12.10 | 3.03 |
| $FeVO_4$ film; 500 °C, 60 min; $d = 90$ nm | | | | | | | | | | | | | | |
| Ex situ IR absorbance spectra | | | | | | | | | CV, scan rate = 5 mV $s^{-1}$ | | | | | |
| Techn | Cycle | $E$ | $i$ | $t$ | $Q_{ins}$ | $Q_{ins}d^{-1}$ | $\rho$ | $x$ | | $E$ | $Q_{ins}$ | $Q_{ins}d^{-1}$ | $x$ | |
| CE | 1 | – | 35.0 | 143 | –5.0 | –0.06 | 3.65 | 0.27 | | –0.26 | –2.1 | –0.02 | 0.11 | |
| | 2 | | | 286 | –10.0 | –0.11 | | 0.54 | | –0.50 | –11.3 | –0.13 | 0.61 | |
| | 3 | | | 286 | –10.0 | –0.11 | | 0.54 | | | | | | |
| | 4 | | | 429 | –15.0 | –0.17 | | 0.81 | | –0.56 | –13.5 | –0.15 | 0.73 | |
| | 5 | | | 429 | –15.0 | –0.17 | | 0.81 | | | | | | |
| | 1 | | 32.1 | 624 | –20.0 | –0.22 | | 1.08 | | –0.83 | –20.8 | –0.23 | 1.11 | |
| | 2 | | | 936 | –30.0 | –0.33 | | 1.62 | | –1.50 | –30.8 | –0.34 | 1.66 | |
| | 3 | | | 1248 | –40.0 | –0.44 | | 2.16 | | –1.04 | –31.8 | –0.35 | 1.72 | |
| $InVO_4$ film; 500 °C, 60 min; $d = 230$ nm | | | | | | | | | | | | | | |
| Ex situ IR absorbance spectra | | | | | | | | | CV, scan rate = 5 mV $s^{-1}$ | | | | | |
| Techn | Cycle | $E$ | $i$ | $t$ | $Q_{ins}$ | $Q_{ins}$d$^{-1}$ | $\rho$ | $x$ | | $E$ | $Q_{ins}$ | $Q_{ins}d^{-1}$ | $x$ | |
| CE | 1 | – | 22.3 | 224 | –5.0 | –0.02 | 4.607 | 0.11 | | –1.00 | –2.9 | –0.01 | 0.07 | |
| | 2 | | | 448 | –10.0 | –0.04 | | 0.23 | | –1.20 | –10.3 | –0.05 | 0.21 | |
| | 3 | | | 896 | –20.0 | –0.09 | | 0.43 | | | | | | |
| | 4 | | | 1344 | –30.0 | –0.13 | | 0.67 | | –1.60 | –36.9 | –0.16 | 0.83 | |
| | 5 | | | 1344 | –30.0 | –0.13 | | 0.67 | | | | | | |
| | 6 | | | 1792 | –40.0 | –0.17 | | 0.90 | | –1.20 | –43.9 | –0.19 | 0.99 | |

[a]Techn: electrochemical technique; CV: cyclic voltammetry; CC: chronocoulometry; CE: chronopotentiometry; *SR*: scan rate; *d*: thickness (nm); *E*: potential (V); *i*: current density (μA $cm^{-2}$); *t*: time (s); $Q_{ins}$: inserted charge density (mC $cm^{-2}$); $Q_{ins}d^{-1}$ (mC $cm^{-2}$ $nm^{-1}$); $x'$: in $Li_{x'}Fe_2V_4O_{13}$; $x$: intercalation coefficient per V atom; $\rho$: density (g $cm^{-3}$)

XRD (Fig. 1, Table 1). The broad bands that characterize the IR spectra of films obtained at 300 °C reflect their predominantly amorphous composition, while for films heated at 400 °C we can establish mixed $FeVO_4$-I and $FeVO_4$-II phases from the increased sharpness and number of IR bands. The crystalline $FeVO_4$-I films (500 °C) exhibit an additional splitting of the IR bands (Fig. 5c).

Vibrational modes were assigned as V-O terminal (range I), V-O···Fe and V···O···Fe bridging (ranges II and III) and V-O-V deformational (range IV) modes (Table 3), while $FeO_5$ and $FeO_6$ modes cannot be ascertained. Such an approximation was made on the basis of the assignment of lead vanadate glasses by Hayakawa et al. [40]. These glasses exhibit vibrational spectra that are very similar to the spectra of amorphous $FeVO_4$ films (300 °C). Their assignment is based on the assumption that glasses consist of $(VO_3)_n$ chains formed by corner-sharing $VO_4$ groups with V-O bonds of different strengths. Stronger V-O bonds bring about modes in range I (V-O terminal stretching), while the V-O-V bridging stretching modes (range II) originate from $VO_4$ groups linked via their corners. In the crystalline $FeVO_4$-I films, $VO_4$ groups do not form chains among themselves, which means that the description of modes as V-O-V bridging loses its meaning and must be replaced by the bridging V-O···Fe and V···O···Fe modes of the stronger and weaker V-O-Fe contacts.

In this case, V-O modes can be assigned according to the molecular modes ($v_1$, $v_2$, $v_3$ and $v_4$) of the undistorted $VO_4^{3-}$ ion that exhibits a $v_1$ totally symmetric stretching mode at 840 $cm^{-1}$, while the triply degenerate $F_2$ stretching appears at 790 $cm^{-1}$ [41]. Alternatively, the structure of $M^{3+}VO_4$ ($M^{3+}$ = Fe, In) can be considered as an ionic compound consisting of isolated $VO_4^{3-}$ anions and $Fe^{3+}$ species. In the crystalline state the $v_3$ mode shifts and splits because the $VO_4$ groups have different V-O bonds. For example, the greatest splitting is observed for the monoclinic $InVO_4$-I crystals that have two $VO_4$ groups, one with a short V-O bond and another with a long V-O bond (Table 3). The V-O bond lengths in the $FeVO_4$-I phase differ to a much smaller extent.

## Ex situ IR spectra of crystalline $FeVO_4$ films (500 °C)

For ex situ IR spectroelectrochemical measurements we charged the $FeVO_4$-I films galvanostatically to various insertion coefficients $x$ (Figs. 6, 7; Table 2). Although these values do not match exactly those obtained from

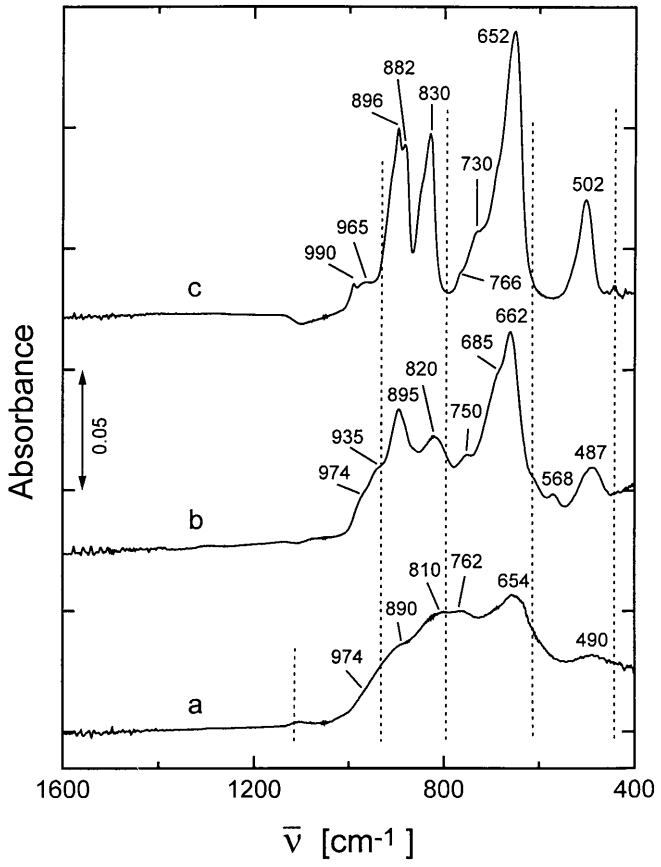


**Fig. 5** IR absorbance spectra of Fe/V (1:1) oxide films heated for 1 h at *a* 300°C, *b* 400 °C and *c* 500 °C ($FeVO_4$)

the first CV of the $FeVO_4$-I film (Fig. 2), they do allow us to ascribe the vibrational band changes to certain current peaks. The first charging to $x = 0.27$, corresponding to the current shoulder at –0.2 V vs. Ag/AgCl (Fig. 2), results in a simultaneous decrease in the intensity of all IR bands without changing their frequencies (Fig. 6A). Discharging reproduces the IR spectrum of the initial film (Fig. 7A), which indicates the reversibility of charging. The second charging ($x = 0.54$) encompasses the most intense current peak at –0.4 V vs. Ag/AgCl (Fig. 2). It results in red frequency shifts of the V-O terminal stretching (range I) and V-O···Fe bridging stretching (range II), while the V···O···Fe bridging mode at 652 $cm^{-1}$ shifts to 696 $cm^{-1}$ (Fig. 6A). However, the initial spectrum is regained after discharging (Fig. 7A). The repeated charging to $x = 0.54$ assesses the identical spectral changes and confirms that no eventual relaxation of the film's structure after repeated charging/discharging occurs. After the fourth charging to $x = 0.81$ (Fig. 6A), which corresponds to the small current peak at –0.55 V vs. Ag/AgCl ($x = 0.73$) in Fig. 2, we no longer observe the splitting of the V-O terminal and V-O···Fe bridging modes and a continuous absorption appears instead (Fig. 6A). Discharging (Fig. 7A) produces a spectrum containing modes characteristic for the third charged spectra (Fig. 6A).

Charging to $x = 1.08$ (Fig. 6B), corresponding to the current peak at –0.6 V vs. Ag/AgCl ($x = 1.11$) in Fig. 2, signals a decrease in the 850 $cm^{-1}$ mode (V-O···Fe bridging) and an increase in the intensity of the $Li^+$-O absorption below 500 $cm^{-1}$, indicating the irreversible uptake of lithium ions [42, 43]. The charging to $x = 1.62$ decreases the intensity of the V-O···Fe bridging mode (864 $cm^{-1}$), while the mode at 420 $cm^{-1}$ increases considerably (Fig. 6B). This charging corresponds to a current peak at approximately –1.0 V vs. Ag/AgCl (Fig. 2). The most pronounced difference between the IR spectra of highly charged and discharged states (Figs. 6B, 7B) is the intensity variation of the absorption below 500 $cm^{-1}$.

**Table 3** Assignment of IR bands of Fe/V (1:1) oxide films prepared at various temperatures together with the variation of the lowest frequency band of $VO_4$ groups in various $M^{3+}$ orthovanadates and V-O bond lengths

| IR bands ($cm^{-1}$) | | Fe:V = 1:1 films | | | Ref |
|---|---|---|---|---|---|
| Range | Assignment | 300 °C | 400 °C | 500 °C | |
| I: 1050–880 $cm^{-1}$ | V-O terminal stretching | 974<br>890 | 970<br>937<br>895 | 990<br>959<br>897<br>884 | – |
| II: 880–700 $cm^{-1}$ | Bridging V-O···Fe stretching | 810<br>762 | 820<br>751<br>684 | 830<br>766<br>728 | – |
| III: 700–550 $cm^{-1}$ | Mixed bridging V-O···Fe and V···O···Fe stretching | 654 | 660<br>570 | 652 | – |
| IV: < 550 $cm^{-1}$ | V-O-V deformation, Fe-O stretching | 490 | 486 | 503 | – |
| $M^{3+}$ orthovanadates | | V-$O_{min}$ (nm)[a] | V-$O_{max}$ (nm)[a] | V-O-V ($cm^{-1}$)[a] | |
| $InVO_4$-I | Monoclinic | 0.159<br>0.164 | 0.187<br>0.178 | 629 | [34] |
| $InVO_4$-III | Orthorombic | 0.1662 | 0.1791 | 723 | [41] |
| $FeVO_4$-I | Triclinic | 0.1649 | 0.1809 | 651 | [32] |
| $FeVO_4$-II | Orthorombic | 0.1652 | 0.1792 | – | [38] |
| $Fe_2V_4O_{13}$ | Monoclinic | 0.153 | 0.188 | 617 | [39] |
| $CeVO_4$ | Tetragonal (wakefieldite) | 0.169 | | 769 | [23] |

[a]V-$O_{max}$, V-$O_{min}$: maximum or minimum length of the V-O bond; V-O-V: bridging V-O-V mode

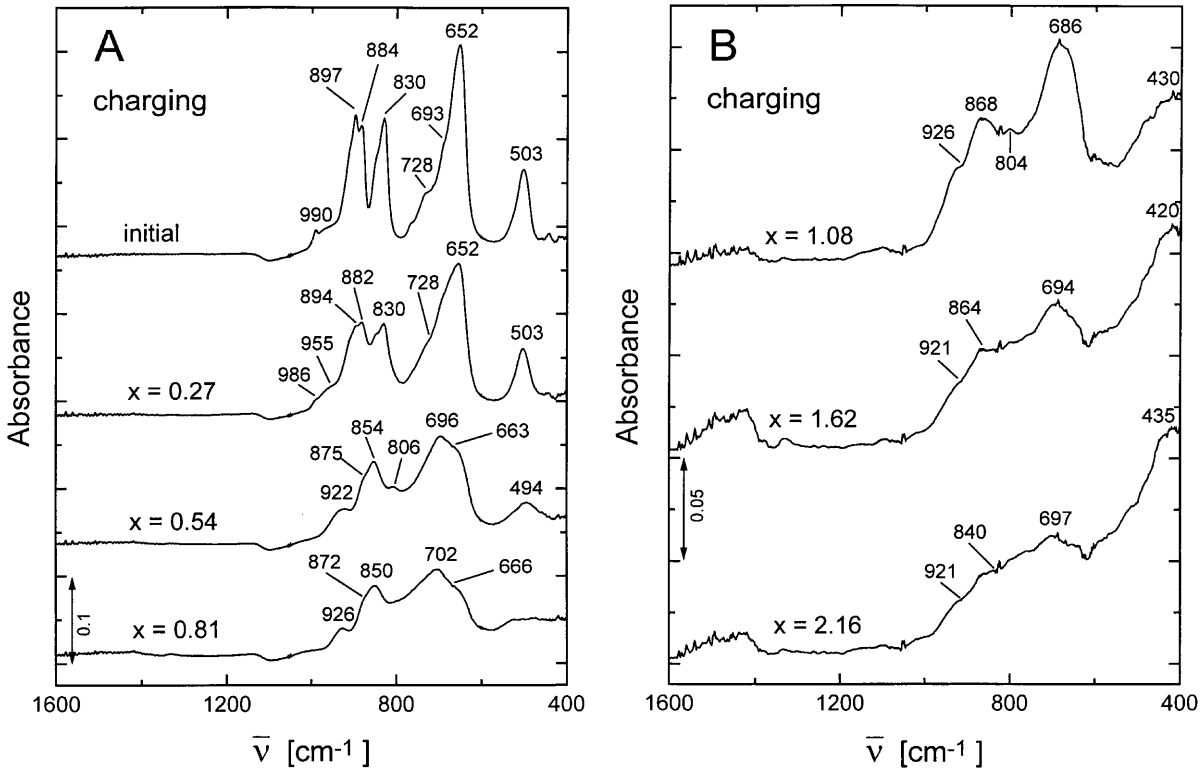


**Fig. 6** Ex situ IR absorbance spectra of a $FeVO_4$ film (500 °C): **A** initial state and charging to $x = 0.27$, 0.54 and 0.81; **B** charging to $x = 1.08$, 1.62 and 2.16

**Fig. 7** Ex situ IR absorbance spectra of a $FeVO_4$ film (500 °C): **A** initial state and discharging from $x = 0.27$, 0.54 and 0.81; **B** discharging from $x = 1.08$, 1.62 and 2.16

## Discussion

Our main goal is to generalize the IR vibrational band changes observed in ex situ IR spectra of $FeVO_4$ crystalline films by comparing them with those

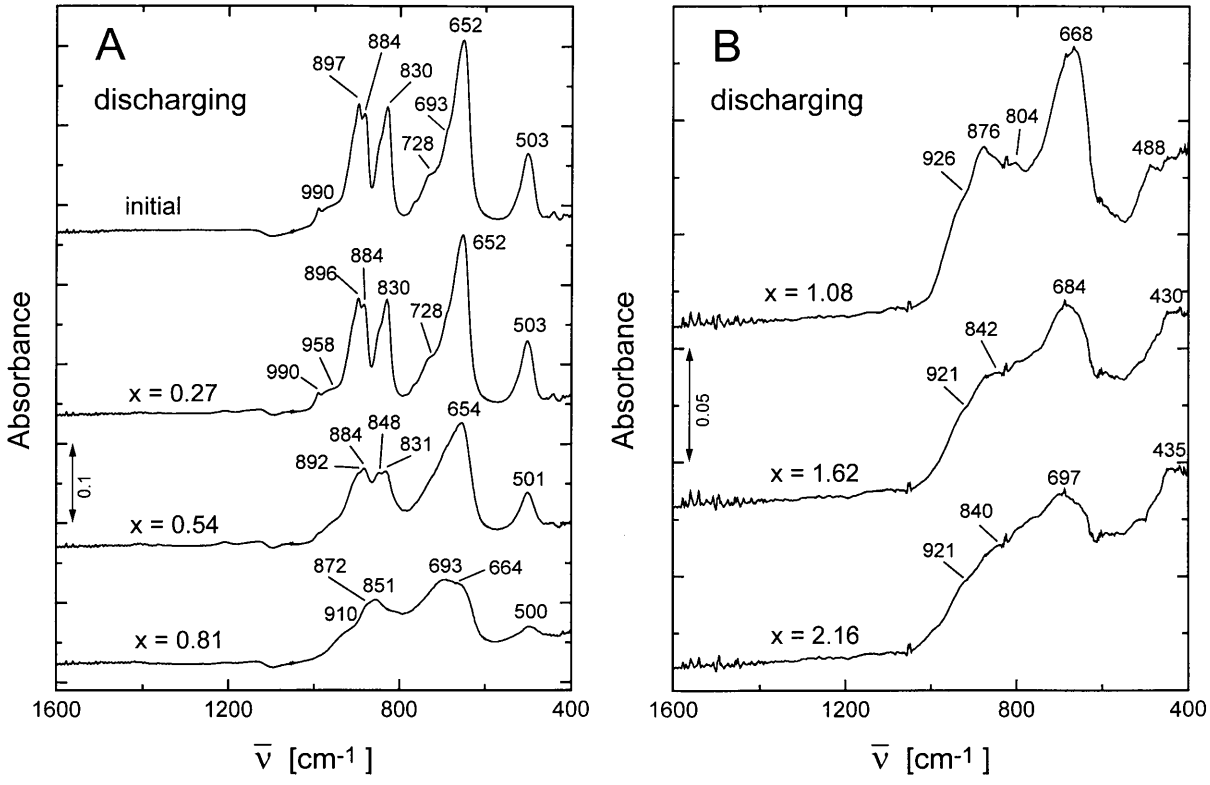

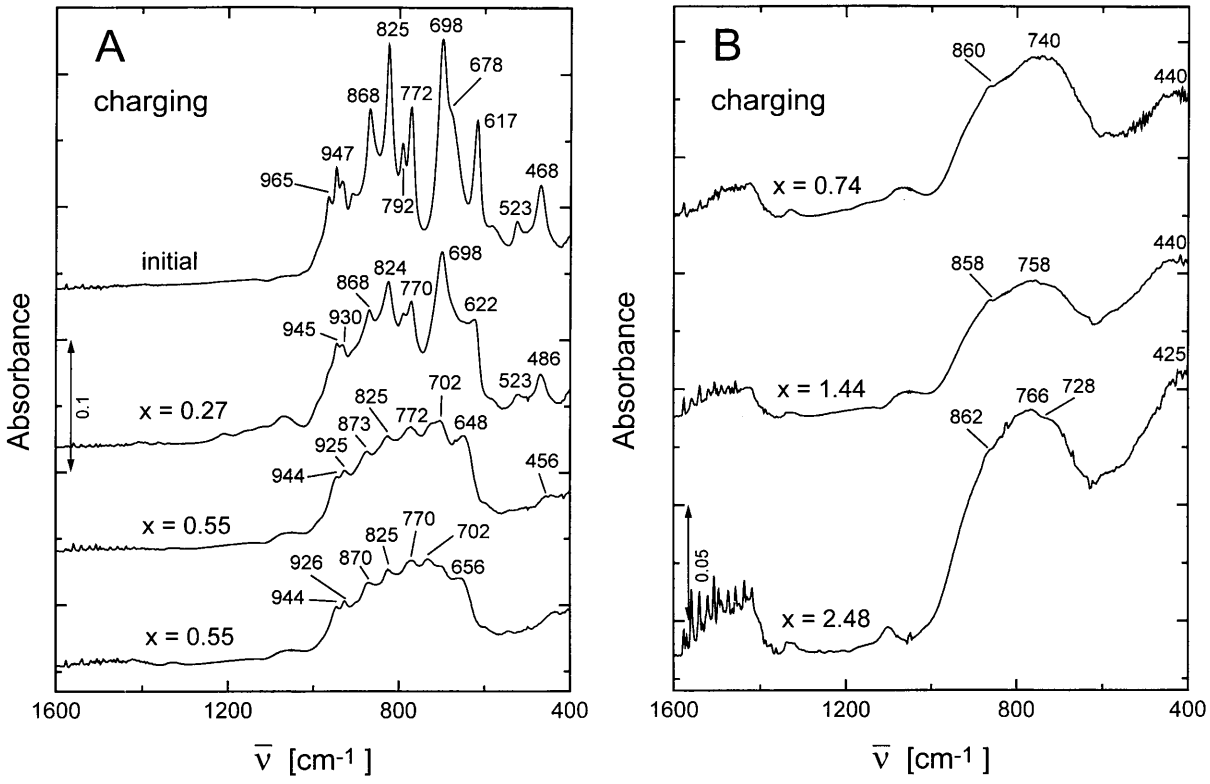


**Fig. 8** Ex situ IR absorbance spectra of a $Fe_2V_4O_{13}$ film (400 °C): **A** initial state and charging to $x=0.27$ and 0.55; **B** charging to $x=0.74$, 1.44 and 2.48

**Fig. 9** Ex situ IR absorbance spectra of a $Fe_2V_4O_{13}$ film (400 °C): **A** initial state and discharging from $x=0.27$ and 0.55; **B** discharging from $x=0.74$, 1.44 and 2.48

observed during the charging/discharging of crystalline $Fe_2V_4O_{13}$ (Figs. 8, 9) and $InVO_4$ (Figs. 10, 11) films. For ex situ IR spectroelectrochemical measurements, films were charged either galvanostatically or potentiostatically and details are given in Table 2. The charges attained during ex situ measurements were

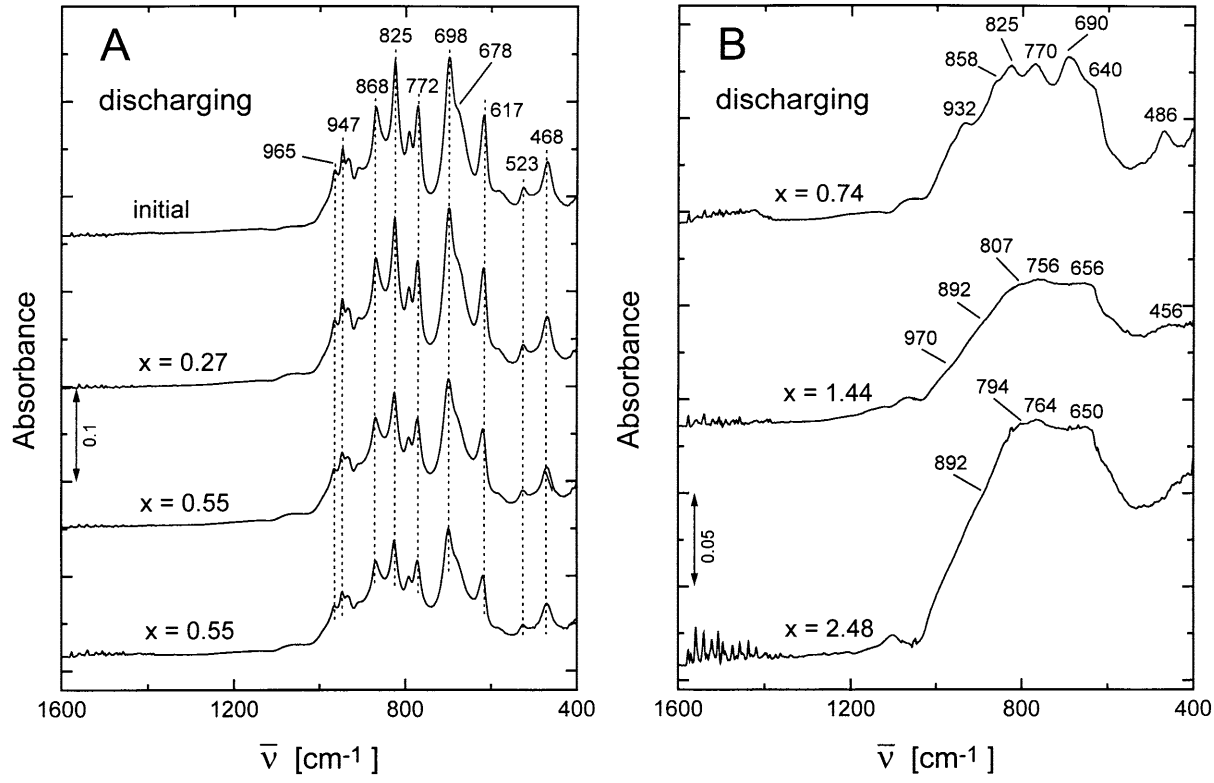

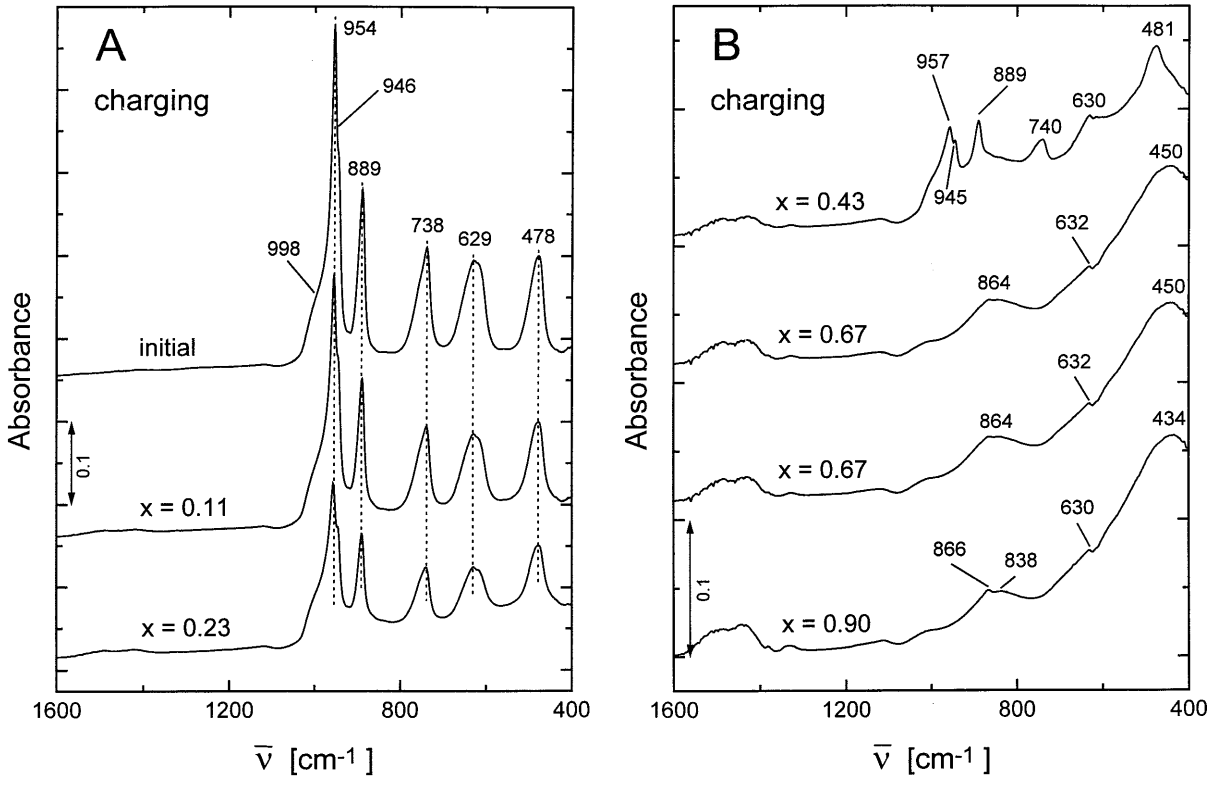


**Fig. 10** Ex situ IR absorbance spectra of an $InVO_4$ film (500 °C): **A** initial state and charging to $x = 0.11$ and 0.23; **B** charging to $x = 0.43$, 0.67 and 0.90

**Fig. 11** Ex situ IR absorbance spectra of an $InVO_4$ film (500 °C): **A** initial state and discharging from $x = 0.11$ and 0.23; **B** discharging from $x = 0.43$, 0.67 and 0.90

compared to those calculated from the first CV response of the corresponding films (Figs. 2, 3, 4) in order to find the connections between the appearance of the current peaks and the IR spectral changes. Inspection of the ex situ IR spectra (Fig. 6, 7, 8, 9, 10, 11) reveals that the IR vibrational band changes are

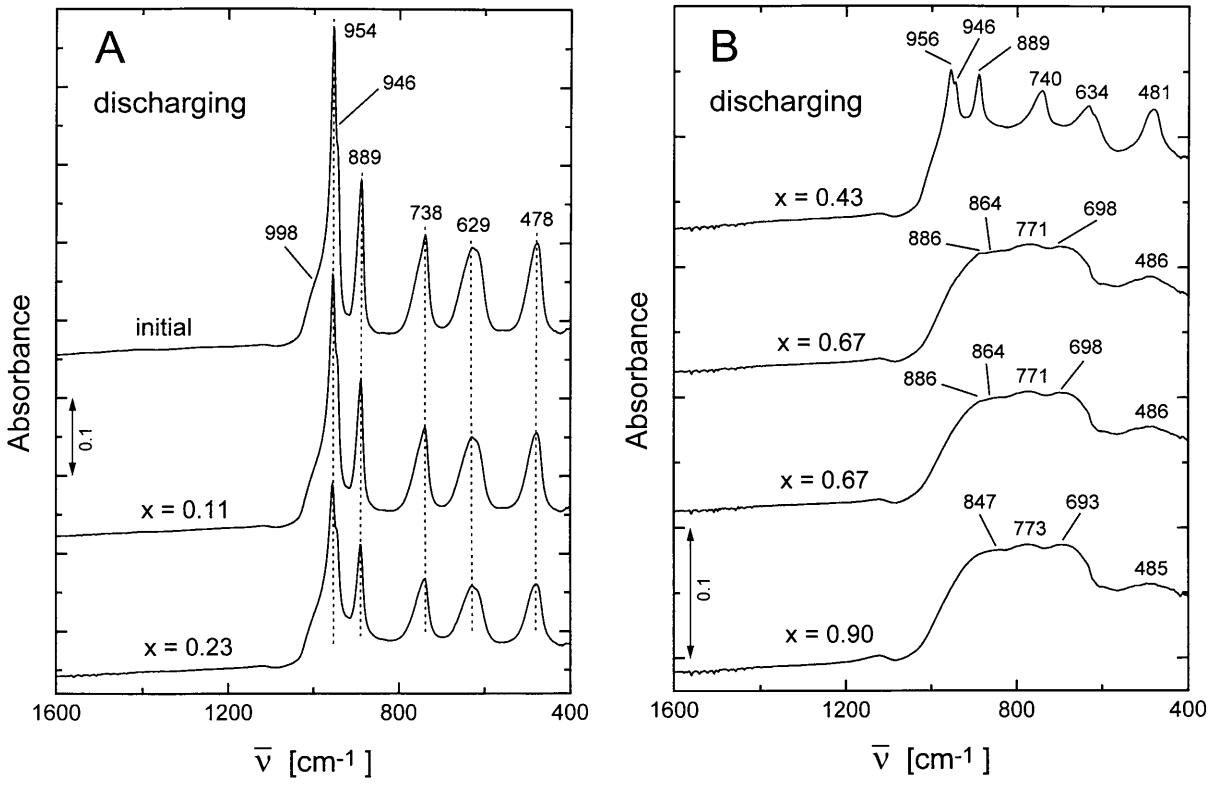

common to all films and enables us to rank the IR spectra into three classes (Fig. 12).

Class I encompasses ex situ IR spectra which show a simultaneous decrease in the intensity of all bands, although their frequencies remained unaltered (Figs. 6, 7, 8, 9, 10, 11, 12; Table 2). The retention of lithium in discharged spectra is not seen and there are no $Li^+$-O interactions that reflect the frequency changes of the bands. This class of spectra signals the complete reversibility of the insertion/extraction reactions. The charging limit is –0.06 and –0.04 mC $cm^{-2}$ $nm^{-1}$ for $FeVO_4$ and $InVO_4$, while it is higher for $Fe_2V_4O_{13}$, i.e. –0.13 mC $cm^{-2}$ $nm^{-1}$ (Table 2).

Class II form ex situ IR spectra which in the charged state exhibit small but distinct red shifts in the V-O terminal stretching and blue shifts of the bridging V-O···$M^{3+}$ stretching modes (Figs. 6, 7, 8, 9, 10, 11, 12; Table 2). These changes are accompanied by an increase in the intensity of the background absorption below 500 $cm^{-1}$, signaling the irreversible lithiation of the films. Films charged to this level show stronger $Li^+$-O interactions, reflected in the band shifts; however, after discharging, spectra similar to the spectra of the initial films can be obtained.

Class III comprises ex situ IR spectra of highly changed films. Strong skeletal modes between 1000 and 500 $cm^{-1}$ diminish in intensity and become substituted by band(s) between 800 and 600 $cm^{-1}$. The most pronounced change is the appearance of a new band between 500 and 400 $cm^{-1}$, superimposed on the strong background absorption. The band is ascribed to the V-O-V (in the case of $Fe_2V_4O_{13}$) or V-O-$M^{3+}$ ($M^{3+}$ = Fe, In) bridging stretching of vanadium in the reduced state (4+ or mixed 3+/4+), while the background absorption corresponds to the $Li^+$-O modes. IR spectra of discharged films (Figs. 7, 9, 11) resemble those of the films obtained at lower temperatures (Fig. 5),

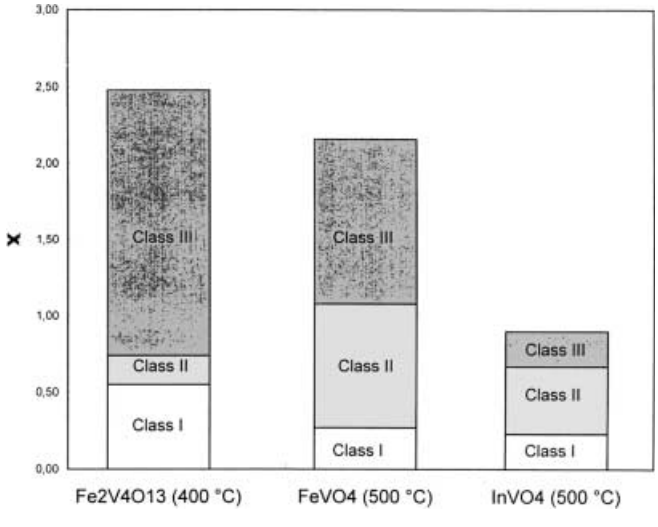


**Fig. 12** Classification of ex situ IR absorbance spectra according to their vibrational band changes

which are amorphous according to the TEM and XRD measurements.

It is difficult to explain the observed changes in class I spectra because the electrochemical insertion of lithium ions usually leads to small shifts of the bands and a decrease in the intensity. A typical example is crystalline $V_2O_5$, which shows a red frequency shift of the V=O (vanadyl) stretching mode (1013 to 1003 $cm^{-1}$) and a diminution in the intensity of the V-O-V bridging mode at 800 $cm^{-1}$ [14, 15]. It is possible to correlate the variations in the band intensity (expressed in absorption coefficient $\alpha$) with the electrical resistivity of films charged to a different extent according to:

$$\alpha(\omega) = 2\pi\sigma(\omega)/nc \quad (1)$$

where $\sigma(\omega)$ represents the electrical conductivity, $n$ the refractive index at high (optical) frequencies $\omega$, and $c$ the velocity of light [44]. For example, for $CeVO_4$ films a linear relationship was found between the electrical resistivity obtained from impedance spectra [45] and the absorption coefficient $\alpha$ of the 790 $cm^{-1}$ band in the $0.3 < x < 2$ domain [23, 28].

Therefore, the reversible drop of the band intensities in the spectra of $FeVO_4$, $InVO_4$ and $Fe_2V_4O_{13}$ films (Figs. 6, 8, 10) can be explained by assuming that electrons entering the films become localized on the bonds exhibiting V-O terminal and bridging V-O···$M^{3+}$ ($M^{3+}$ = Fe, In) stretching vibrations. The simultaneous decrease in the intensity of all the bands means that the polarity of all V-O bonds varies to the same extent. More bound electrons are not accessible for polaron hopping, which is reflected in the weak polaron absorption of all the investigated films.

Class II comprises spectra that show a transition from the crystalline to the amorphous state and these spectra signal the differences in the extent to which vanadium is reduced. Spectra ranked in class III represent the amorphous state of the films, which we conclude from the close resemblance of spectra of discharged films (Figs. 7, 9, 11) to the spectra of the initial films obtained at lower temperatures (Fig. 5) [25, 26, 27, 28, 29] and to the spectra of lead vanadate glasses [40]. The absence of the vanadyl (V=O) stretching mode above 1000 $cm^{-1}$ and three V-$O_C$ stretching modes between 450 and 480 $cm^{-1}$ in lead vanadate glasses [40] rules out the presence of $VO_5$ trigonal bipyramids also in the spectra of our discharged films. A comparison of the spectra of discharged films (Figs. 7, 9, 11) with those of initially amorphous films (Fig. 5) [25, 26, 27, 28, 29] shows small differences in the band frequencies. This indicates the presence of $V^{4+}$ species which remain in the discharged films. In addition, the higher intensity of the background absorption below 500 $cm^{-1}$ shows the presence of lithium ions in the discharged films (Figs. 7, 9, 11). The crystalline $FeVO_4$, $InVO_4$ and $Fe_2V_4O_{13}$ films attain amorphization at different $x$ values. The highest charging is needed for the amorphization of $Fe_2V_4O_{13}$ ($x = 1.44$) and $FeVO_4$ ($x = 1.62$)

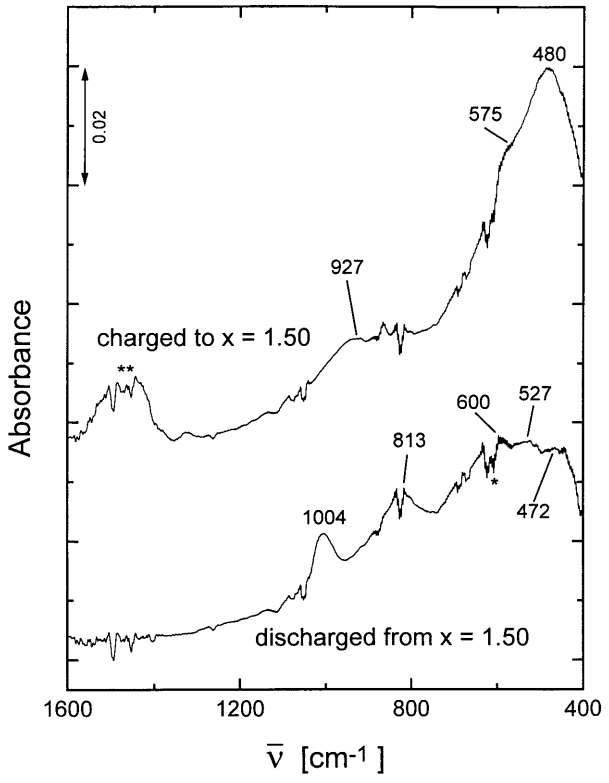


**Fig. 13** Ex situ IR absorbance spectra of a crystalline $V_2O_5$ film (300 °C) charged/discharged to $x = 1.5$ ($x$ per V atom); * and ** denote $CO_2$ and carbonate vibrations

films. The crystalline $InVO_4$ films attain the transformation at $x = 0.67$.

Two bands which appear in the highly charged spectra (Figs. 6, 8, 10) consist of the weaker one in the range of the skeletal V-O and V-O···$M^{3+}$ ($M^{3+}$ = In, Fe) modes and a stronger band superimposed on the broad $Li^+$-O absorption below 500 $cm^{-1}$. The latter undoubtedly corresponds to the skeletal modes of $V^{4+}$ or $V^{3+}$ species vibrating against the oxygen host. To prove the nature of this band we repeatedly charged crystalline $V_2O_5$ films in the $0 < x < 1.5$ domain ($x$ in $Li_xVO_{2.5}$). For charging to $x = 1.5$ the $V_2O_5$ spectrum reveals similar IR vibrational band structure below 500 $cm^{-1}$; however, the weaker band appears between 950 and 900 $cm^{-1}$ (Fig. 13). This is expected because the amorphous $Li_xVO_{2.5}$ phase still contains vanadyl V = O bonds which shift from 1013 $cm^{-1}$ to lower values.

## Conclusions

Ex situ IR spectroelectrochemical investigation of charged films is an effective way to assess structural transformation. The reversible intensity variations of IR bands with charging open up new possibilities to correlate IR spectral changes with the electrical resistivity of films charged to various extents.

**Acknowledgements** The authors thank the Ministry for Science and Technology of Slovenia for their financial support.

## References

1. Suëtaka W (1995) Surface infrared and Raman spectroscopy, methods and application. Plenum Press, New York
2. Ashley K (1990) Spectroscopy 5:22
3. Ashley K, Pons S (1988) Chem Rev 88:673
4. Neugebauer H, Moser A, Strecha P, Neckel A (1990) J Electrochem Soc 137:1472
5. Tschinkel W, Neugebauer H, Neckel A (1990) J Electrochem Soc 137:1475
6. Trettehahn GLJ, Nauer GE, Neckel A (1993) J Power Sources 42:137
7. Goren E, Chusid (Youngman) O, Aurbach D (1991) J Electrochem Soc 138:L6
8. Aurbach D, Chusid (Youngman) O (1993) J Electrochem Soc 140:L1
9. Aurbach D, Daroux ML, Faguy PW, Yeager E (1987) J Electrochem Soc 134:1611
10. Ichino T, Cahan BD, Scherson DA (1991) J Electrochem Soc 138:L59
11. Aurbach D, Gamolsky K, Markowsky B, Calitza G, Gofer Y, Heider V, Oesten R, Schmidt M (2000) J Electrochem Soc 147:1322
12. Wen SJ, Richardson TJ, Ma L, Striebel KA, Ross PN, Cairns EJ (1996) J Electrochem Soc 143:L136
13. Neckel A (1987) Mikrochim Acta 3:263
14. Šurca A, Orel B, Dražič G, Pihlar B (1999) J Electrochem Soc 146:232
15. Šurca A, Orel B (1999) Electrochim Acta 44:3051
16. McIntyre JDE, Aspens DE (1971) Surf Sci 24:417
17. Harbecke B, Heinz B, Grosse P (1985) Appl Phys A 38:263
18. Grosse P (1990) Vibrational Spectrosc 1:187
19. Neugebauer H, Ping Z (1997) Mikrochim Acta (Suppl) 14:125
20. Johnson BW, Pettinger B, Doblhofer K (1993) Ber Bunsenges Phys Chem 97:412
21. Johnson BW, Bauhofer J, Doblhoffer K, Pettinger B (1992) Electrochim Acta 37:2321
22. Christensen PA, Hammett A, Hillman AR, Swann MJ, Higgins SJ (1992) J Chem Soc Faraday Trans 88:595
23. Opara Krašovec U, Orel B, Šurca A, Bukovec N, Reisfeld R (1999) Solid State Ionics 118:195
24. Šurca A, Benčič S, Orel B, Pihlar B (1999) Electrochim Acta 44:3075
25. Šurca A, Orel B, Opara Krašovec U, Lavrencic Štangar U, Dražič G (2000) J Electrochem Soc 147:2358
26. Bencic S, Orel B, Šurca A, Lavrencic Štangar U (2000) Solar Energy 68:499
27. Šurca A, Orel B, Dražič G, Decker F, Colomban P (2001) J Sol-Gel Sci Technol (in press)
28. Šurca Vuk A, Opara Krašovec U, Orel B, Colomban P (2001) J Electrochem Soc (in press)
29. Orel B, Šurca Vuk A, Opara Krašovec U, Dražič G (2001) Electrochim Acta 46:2059
30. Denis S, Baudrin E, Touboul M, Tarascon JM (1997) J Electrochem Soc 144:4099
31. Touboul M, Tolédano P (1980) Acta Crystallogr Sect B 36:240
32. Robertson B, Kostiner E (1972) J Solid State Chem 4:29
33. Touboul M, Melghit K, Bénard P (1994) Eur J Solid State Inorg Chem 31:151
34. Roncaglia DI, Botto IL, Baran EJ (1986) J Solid State Chem 62:11
35. Touboul M, Popot A (1985) Rev Chem Miner 22:610
36. Baudrin E, Denis S, Orsini F, Seguin L, Touboul M, Tarascon JM (1999) J Mater Chem 9:101
37. Stadelmann PA (1987) Ultramicroscopy 21:131
38. Oka Y, Yao T, Yamamoto N, Ueda Y, Kawasaki S, Azuma M, Takano M (1996) J Solid State Chem 123:54
39. Permer L, Laligant Y (1997) Eur J Solid State Inorg Chem 34:41

40. Hayakawa S, Yoko T, Sakka S (1995) J Non-Cryst Solids 183:73
41. Baran EJ, Escobar ME (1985) Spectrochim Acta 41A:415
42. Proudhomme, Tarte P (1972) Spectrochim Acta 28A:69
43. Tarte P (1964) Spectrochim Acta 20:238
44. Colomban Ph, Badot JC (1992) Frequency dependent conductivity, microwave dielectric relaxation and proton dynamics. In: Colomban Ph (ed) Proton conductors, solids, membranes and gels – materials and devices. (Chemistry of solid state materials 2) Cambridge University Press, Cambridge, p 391
45. Picardi G, Varsano F, Decker F, Opara Krašovec U, Šurca A, Orel B (1999) Electrochim Acta 44:3157